Antipodal seismic observation locates liquid region on the Earth's Inner Core

Seiji Tsuboi (tsuboi@jamstec.go.jp)
Japan Agency for Marine-Earth Science and Technology https://orcid.org/0000-0003-3422-6879
Rhett Butler
University of Hawaii at Mānoa https://orcid.org/0000-0002-1796-2797

Article

Keywords:

Posted Date: May 12th, 2022

DOI: https://doi.org/10.21203/rs.3.rs-1555970/v1

Abstract

The Earth's inner core is thought to have been formed by the precipitation of iron from the fluid outer core[1]. It is considered that a part of the inner core surface where iron in the fluid outer core is precipitated may be melted and formed a mushy region[2-4], but its position is not well understood seismologically. We recently analyzed seismic waveforms observed at the antipodal station of the seismic source and showed that there may be a clear precursor of lower reflections at the inner core boundary[5]. It has been found that this precursor wave can be successfully modeled as a reflection under the liquid / solid interface at a depth of 100 km below the inner core boundary. In this study, we use these precursor waves of the lower reflection at the inner core boundary observed at the antipodal station (> 179°). The sensitivity kernel for the shear wave velocity structure on the inner core surface was calculated by the adjoint method corresponding to these precursor waves, using theoretical seismic waveforms. The location of the fluid region was identified using the obtained sensitivity kernel. Our results show two regions of the inner core surface where the shear wave velocity is close to zero and is considered fluid. These regions are consistent with the westward shifts of geomagnetic anomalies observed on the Earth's surface and the regions of upwellings expected from geomagnetic dynamo simulations in the outer core[3]. These results may provide a seismological evidence that the inner core is locked to the mantle through the geodynamic motion in the outer core and provide new insights to the origin of the earth's magnetic field.

Full Text

When the seismic wave is recorded at the antipodal point of an earthquake ($\Delta \simeq 180°$), this seismic wave is focused near the antipodal point where the seismic energy is amplified, excepting only paths traversing a diameter through the earth, i.e., the PKIKP wave. The surface of the wave field that makes up the seismic propagation to the antipodal point surrounds the earth in an annular region around the diameter between the epicenter and the antipodal point. Various studies have been conducted on the Earth's inner core structure using these characteristic properties[6–13].

Antipodal seismic observation

In this study, we use data from earthquake in Tonga to station in Algeria (TAM), Sulawesi to Amazon (PTGA), northern Chile to Hainan Island (QIZ), and central Chile to mainland China (ENH, and XAN), studied in Butler and Tsuboi (2021)[5]. In addition to these earthquake-receiver pairs, we also examined Spanish data (ECAL) from an earthquake in New Zealand. Figure 1 shows raypaths of PKIKP and PKIIKP waves, each epicenter, and the antipodal observation point, and Table S1 shows the hypocenter information of the earthquake used. Figure 2 shows each of the seismic waveform data used to derive sensitivity kernels. Waveform data from TAM and PTGA show that there is a significant arrival between PKIIKP and PKIIKP, about 7 and 17 seconds before PKIIKP. In contrast to TAM and PTGA data, for Chinese stations (QIZ, ENH, XAN), no arrival of this waveform is seen . Taking into account that the propagation paths of these waves do not share a common path in the crust, mantle, and outer core, Butler and Tsuboi

(2021)[5] applied stacking to these observations to improve the signal-to-noise ratio, which includes amplitude and phase weighted stacking[14] as well as slant stacking along ray parameters[8]. Figure 2 indicates approximate boundaries between observation points with large seismic arrivals (TAM, PTGA, and ECAL) between PKIKP and PKIIKP and small ones (XAN, ENH, and QIZ). These results show two groups: TAM, PTGA, and ECAL with a clear PKIIKP precursor, and QIZ, ENH, XAN with no visible precursor.

Butler and Tsuboi (2021)[5] show that the precursors of PKIIKP waves observed at these antipodal stations can be successfully modeled as reflected below a liquid/solid interface at a depth of 100 km below the inner core boundary. The boundaries we have shown are highly reflective and sensitive to shear wave velocity contrasts above 5 km/s. Butler and Tsuboi (2021)[5] show that the earlier precursory waves observed by TAM and PTGA may be modeled as a clear discontinuity near the depth of about 250 km below the inner core surface. Assuming that the energy between PKIIKP and PKIKP propagates deeper and faster through the inner core than PKIIKP, the precursor wave is tentatively called PKI_{100}IKP, reflecting the uncertain origin in the inner core. The PKI_{100}IKP boundary proposed here needs to consider the three dimensional structure at the top of the inner core in order to match the orthogonal paths of the TAM and ENH data at the same time.

Sensitivity kernels by adjoint method

In this paper, we calculated the sensitivity kernel of shear wave velocity to be used in the waveform inversion using the liquid/solid boundary of S wave velocity 100 km below the surface of the inner core as an initial model, and tried to identify the position of the fluid region on the surface of the inner core. Although the number of earthquakes used is not large, the raypaths of PKIIKP phase covers the surface of the inner core in annulus manner. Each of the earthquake-receiver pairs used in this study covers a ray-surface encompassing nearly 60% of the inner core surface—the orthogonal, antipodal propagation surfaces of TAM and ENH together encompass the whole of the top of the inner core (Butler and Tsuboi, 2010)[9].

To calculate the sensitivity kernels, we use the 3D spectral element method (3DSEM) [15–18], as in our previous studies[9,12,13]. The Earth's internal structure model used incorporates a 3D tomography model (s362wmani)[19] for the Earth's mantle, a crustal model CRUST2.0[20], and ellipticity. By incorporating the 3D mantle and crust, the energy scattered from the structure above the core (e.g., the upper mantle, D" and the boundary between the core and mantle) is included in the 3DSEM simulation. We calculate the sensitivity kernel of the inner core shear wave structure for the amplitude of precursor waves. In order to do so, we have included a spherically symmetric shear wave structure as: Vs = 0.5 km/s from the inner core surface to a depth of 100 km, Vs = 5.0 km/s from 100 km to 250 km, and a spherically symmetric structure with a PREM model below the depth 250 km (Fig. 1). The spectral element method program, specfem3d_globe, is used, and the 9600 cores of the Earth simulator were utilized to calculate the theoretical seismic waveform with an accuracy of about 8 seconds.

This starting model is derived from Butler and Tsuboi, 2021)[5], who measured highly-reflective regions below the Inner Core Boundary. The waveforms of observed phases precursory to PKIIKP are best matched with a liquid layer overlying a fast shear wave region where Vs ≥ 5 km/s, which significantly exceeds PREM at 3.5 km/s. This high shear wave speed is consistent with *ab initio* calculations (Vočadlo, 2007; Deuss, 2008)[21, 22] and experimental results (Mao et al., 1998)[23] for iron and its alloys at inner core pressure and temperature that can reach Vs > 6 km/s.

The calculation of the finite frequency sensitivity kernel of the inner core shear wave velocity structure was performed by the adjoint method[24-30]. The finite frequency sensitivity kernel calculation is done in two steps (see method for details). First, for the earthquakes shown in Table S1, the hypocenter of the global CMT mechanism[31] is used to calculate the theoretical seismic waveform for the seismic station of the antipodal point corresponding to each earthquake. At this time, the global wave field at the end of the time step in which the theoretical seismic waveform is calculated is saved in the disk. We apply the same band pass filter with a period of 8 seconds and 50 seconds to both theoretical seismograms and observed seismograms. From the calculated seismic waveforms and observed waveforms, we set the time window of arrival of PKIIKP waves and PKI_{100}-IKP waves, and cut out these waveforms (approximately the blue interval in Figure 2). We calculate the adjoint source for the amplitude of the seismic waveform from the difference between the observed waveform and the theoretical waveform. Since the accuracy of the theoretical seismic waveform used here is about 8 seconds, it is not possible to identify the PKIIKP wave and the PKI_{100}-IKP wave independently, so when cutting out the waveform, we set the window to include both of these phases. Then, using the adjoint source obtained in this way, the theoretical seismic waveform that propagates backward from the observation station to the seismic source is calculated by reversing the time. We calculate the finite-frequency kernel of the shear wave velocity for the amplitude of the PKIIKP wave and the PKI_{100}-IKP wave for the path combining the propagation of the seismic waves from the source to the observation station used from the theoretical seismic waveform calculated beforehand.

Figure 3 shows both the theoretical seismic waveform and the observed waveform for the August 16, 2013 earthquake in New Zealand observed at the ECAL station in Spain, and the adjoint source of the amplitude for the PKIIKP and PKI_{100}-IKP waves. A cross-sectional view of the sensitivity kernel of the shear wave velocity structure of the amplitude with respect to the PKI_{100}-IKP wave is shown. From this figure, it can be seen that the amplitudes of the PKIIKP and PKI_{100}-IKP waves are sensitive to the shear wave velocity structure of the incident point and exit point of the inner core surface as these waves pass through the inner core. The adjoint kernel calculated for such an earthquake and its antipodal observation point is called an event kernel. For the twelve seismic source-receiver pairs used here, the event kernel for the shear wave velocity structure was calculated, and the event kernel for the inner core shear wave structure was extracted. By adding the event kernels calculated in this way, the gradient of the misfit function to improve the initial model was calculated.

Location of fluid region at the surface of the inner core

Using the gradient of misfit function, we can find the change δm that updates the model. Here, assuming that the initial model is updated with a step length of 10%, the amount of modification of the model for the shear wave structure of the inner core was calculated. Figure 4 shows the amount of modification of the shear wave velocity structure in the upper 100 km of the inner core. Figure 4 shows that the west coast of South America and the vicinity of Indonesia need to be modified to slow down the shear wave velocity structure near the inner core surface by up to 2% from the initial model. Since the shear wave velocity of the initial model is 0.5 km/s, these locations can be considered as regions of fluid where the shear wave velocity is close to zero. In addition, it has been shown that surrounding these regions construed as fluid there are alterations increasing the shear wave velocity, which may be construed as a region closer to a solid. In full waveform inversion using the sensitivity kernel, once the updates to the initial model are obtained, the inner core shear wave structure is calculated by modifying the model. Then we calculate the sensitivity kernel again, and repeating this process until the difference between the observed waveform and the theoretical waveform is minimized. By iterating this process repeatedly, the 3D variation of the shear wave velocity structure of the inner core can be obtained. However, the amount of modification to the inner core shear wave velocity structure is small in this case, and the initial model used is not very realistic assuming that the inner core surface is almost fluid. Therefore, here, we do not repeat the procedure but we discuss the location of the fluid region at the surface of the inner core surface layer estimated from this modification.

Previous studies have shown little evidence of P-wave discontinuities near depths of 100 km in the inner core[32-35]. Cormier and Attanayake[36] found a 1% Vp discontinuity under 140 km of the ICB, centered under the Atlantic Ocean, but not elsewhere. Complexities such as 3D structure and anisotropy have been clearly expressed in previous P-wave studies[37–39], but the details of the inner core S-wave structure remain unsolved. Butler and Tsuboi (2021)[5] have shown that the precursors of PKIIKP waves observed at the antipodal point can be successfully modeled as reflected below the liquid/solid interface at a depth of 100 km below the inner core boundary. This boundary has high reflectivity and is sensitive to shear wave velocity contrasts of 5 km/s and above. It is suggested that the newly proposed PKI_{100}IKP boundary is not the same everywhere at the surface of the inner core, because the precursors of PKIIKP wave do not appear for the Chinese stations. Therefore, in order to match both TAM and ENH at the same time, it is necessary to consider the heterogenous shear wave velocity structure at the top of the inner core and it is suggested that the fluid region at the top of the inner core should be localized. The two regions where there are possibilities of fluid shown in Fig. 4 coincide with the positions of the upwelling basins localized on the inner core surface shown by Gubbins et al (2011)[3] in the Earth's dynamo simulation. Their geodynamo simulation is assumed to be related to the seismic velocity anomalies at the Core-Mantle Boundary, which are supposed to be linked to the mantle convection. It is intriguing that the completely independent analysis of the seismic waves reflected from the inner core surface, which we proposed in the present paper, yields results suggesting the same regions. Because the flow pattern at the inner core surface derived by the geodynamo simulation is linked to the core mantle boundary through outer core fluid motion, our results suggest that the inner core is locked to the mantle through the geodynamo fluid motion in the outer core. One of the suggested fluid regions at the surface of the inner core also

corresponds to the geomagnetic anomaly observed at the surface of the Earth[40], which was thought to be linked to the anomaly at the core mantle boundary. If the geomagnetic anomaly is also linked to the seismic velocity anomaly at the surface of the inner core, it also may provide an evidence that the inner core is locked to the mantle. The geodynamo simulation shows that there are relatively large areas of negative (melting) and low-positive heat flux on the ICB, and relatively small areas of strong-positive heat flux (freezing). Therefore, the dynamo simulation suggests that the possible fluid region suggested by our study corresponds to a solidified part, which is inconsistent with our results. This may require a different interpretation of the Earth's dynamo mechanism.

In this study, we did not repeat the iteration to obtain 3D shear velocity structure in the inner core because the number of seismic-observation combinations used was small and the amount of modification of the initial model by full waveform inversion was small. The possible fluid regions of the inner core surface suggested in this study may depend on the distribution of seismic sources. Then we need to repeat the iteration by increasing the source-receiver pairs in the future. It is desirable to estimate the shear wave velocity structure of the inner core surface layer three-dimensionally by repeating the waveform inversion using the finite frequency sensitivity kernels.

Method

Computation of the sensitivity kernels based on the adjoint method

In tomographic inversion, we use observed seismograms and synthetic seismograms to compute the misfit between them to improve the Earth model iteratively. The misfit function is

$$\chi(m) = \sum_{s=1}^{N}\sum_{r=1}^{M}\int_{0}^{T}\frac{1}{2}\left|\left|u(x_r, x_s; t) - d(x_r, x_s; t)\right|\right|^2 dt \quad (1)$$

where **d** is the observed waveform at receivers $\mathbf{x_r}$ (r=1, …, M) excited by earthquakes at $\mathbf{x_s}$ (s=1, …, N). **u** is the synthetic seismograms computed for model **m**. To minimize the misfit function iteratively, we need to compute the gradient is to take the derivative of (1) with respect to model parameters; $\partial\chi(m)/\partial m$ .To compute the gradient we need to compute the derivatives for each time step in the time window considered and for all the source-station pairs, which is formidable amount of computation. Tromp et al. (2005) [24] and Tromp et al. (2008) [25] , however, proposed to compute the gradient based on the adjoint method, which uses the wavefield emitted and back-propagated from the receivers. The perturbation of the misfit function can be expressed as:

$$\delta\chi(m) = \sum_{s=1}^{N}\sum_{r=1}^{M}\int_{0}^{T}[u(x_r, x_s; t) - d(x_r, x_s; t)] \cdot \delta u(x_r, x_s; t)dt \qquad (2)$$

where δu is the perturbation of displacement derived by the first-order Born approximation. Then equation (2) can be written as;

$$\delta\chi(m) = -\sum_{s=1}^{N}\int_{V}\left[K_\rho(x, x_s)\delta ln\rho(x) + K_\lambda(x, x_s)\delta ln\lambda(x) + K_\mu(x, x_s)\delta ln\mu(x)\right]d^3x$$

and Fréchet derivatives with respect to the density and Lame parameter are derived by:

$$K_\rho(x, x_s) = -\int_{0}^{T}\rho(x)u^\dagger(x, x_s; T-t) \cdot \partial_t^2 u(x, x_s; t)dt$$

$$K_\lambda(x, x_s) = -\int_{0}^{T}\lambda(x)\nabla \cdot u^\dagger(x, x_s; T-t)\nabla \cdot u(x, x_s; t)dt$$

$$K_\mu(x, x_s) = -2\int_{0}^{T}\mu(x)\nabla \cdot u^\dagger(x, x_s; T-t)\nabla \cdot u(x, x_s; t)dt$$

where

$$u^\dagger(x, x_s; t) = \int_{0}^{t'}\int_{V} G(x, x': t'-t) \cdot f^\dagger(x', x_s; t)d^3x'dt$$

and

$$f^\dagger(x, x_s; t) = \sum_{r=1}^{M}[u(x_r, x_s; T-t) - d(x_r, x_s; T-t)]\delta(x - x_r)$$

where G is the Green's tensor.While, computation of the kernels based on the adjoint\state method needs one forward simulation and one adjoint field simulation, which requires huge amount of disk space and the computational time. Instead, Tromp et al., (2008)[25] and Peter et al (2011)[30] proposed that three simulations can be used to save the computational resources, i.e., perform the forward calculation twice,

once to compute the adjoint sources and once again at the same time as the adjoint simulation to correlate the two fields and sum their interaction on the fly over all the time steps. We use the mesh discretization parameter NEX=640, which generate synthetics with about 8 second accuracy by using 9600 cores of the Earth Simulator. It took about 2 hours computational time to perform the forward simulation and about 3 hours for the backward simulation.

Declarations

Acknowledgments and data availability

This work is partially supported by JSPS KAKENHI Grant Number JP21K03710. Data were obtained from GEOSCOPE and the IRIS Data Management System. We used the computer program (SPECFEM3D) for Spectral-Element Method. We thank Daniel Peter for his assistance in computing sensitivity kernels by adjoint method. All the computations are performed using the Earth Simulator at the Earth Simulator Center of JAMSTEC. Centroid moment tensor solutions (GCMT) are used for synthetic models. We thank GEOSCOPE, USGS and NSF, NCDSN China, and the Spanish Digital Seismic Network for the operation and maintenance of the seismic stations used in this study. All data were downloaded from the IRIS Data Management System and ORFEUS. Earthquake parametric data were downloaded from the USGS earthquake catalog and tabulated in the Supplementary Information file. Earthquake source mechanisms were downloaded from the Global Centroid Moment Tensor database. SOEST contribution number _____ and HIGP contribution number ____.

Authorship contribution statement

Seiji Tsuboi: Methodology, Investigation, Software, Writing – review & editing.

Rhett Butler: Conceptualization, Methodology, Data curation, Visualization, Writing.

Declaration of interests

The authors declare that they have no known competing financial interests or personal relationships that could have appeared to influence the work reported in this paper.

References

1. Biggin, A., Piispa, E., Pesonen, L. et al. Palaeomagnetic field intensity variations suggest Mesoproterozoic inner-core nucleation. *Nature***526**, 245–248 (2015). https://doi.org/10.1038/nature15523
2. Shih, S. A., & Chao, B. F. Inner core and its libration undergravitational equilibrium: Implications to lower-mantle density anomaly. *Journal of Geophysical Research: Solid Earth*, **126**, e2020JB020541. (2021) https://doi.org/10.1029/2020JB020541

3. Gubbins, D., Sreenivasav, B., Mound, J. and Rost, S. Melting of the Earth's inner core. *Nature***473**, 361-363 (2011) https://doi.org/10.1038/nature10068
4. Alboussière, T., Deguen, R. & Melzani, M. Melting-induced stratification above the Earth's inner core due to convective translation. *Nature***466**, 744–747 (2010). https://doi.org/10.1038/nature09257
5. Butler, R., Tsuboi, S., Antipodal seismic reflections upon shear wave velocity structures within Earth's inner core. *Physics of the Earth and Planetary Interiors*, **321**, (2021) 106802, https://doi.org/10.1016/j.pepi.2021.106802.
6. Rial, J.A. and Cormier, V.F., Seismic waves at the epicenter's antipode. *Journal of Geophysical Research: Solid Earth*, **85**(B5), pp.2661-2668. (1980).
7. Butler, R., Amplitudes at the antipode. *Bull. Seismol. Soc. Am.***76**, 1355–1365 (1986).
8. Niu, F., and Chen, QF, Seismic evidence for distinct anisotropy in the innermost inner core. *Nature Geosci.*, **1**, 692–696 (2008). https://doi.org/10.1038/ngeo314
9. Butler, R., and Tsuboi, S., Antipodal seismic observations of temporal and global variation at Earth's inner-outer core boundary. *Geophys. Res. Lett.***37**, L11301. (2010) https://doi.org/10.1029/2010GL042908.
10. Cormier, V.F., Detection of inner core solidification from observations of antipodal PKIIKP. *Geophysical Research Letters*, **42**(18), pp.7459-7466. (2015).
11. Attanayake, J., Thomas, C., Cormier, V. F., Miller, M. S., & Koper, K. D. Irregular transition layer beneath the Earth's inner core boundary from observations of antipodal PKIKP and PKIIKP waves. *Geochemistry, Geophysics, Geosystems*, **19.** (2018) https://doi.org/10.1029/ 2018GC007562
12. Tsuboi, S. and R. Butler, Inner core differential rotation rate inferred from antipodal seismic observations. P*hysics of Earth and Planetary Interiors*, **301**, , 106451, (2020) doi.org/10.1016/j.pepi.2020.106451.
13. Butler, R. and Tsuboi, S., Antipodal observations of global differential times of diffracted P and PKPAB within the D" layer above Earth's core–mantle boundary. *Geophysical Journal International*, **222**(1), pp.327-337. (2020).
14. Schimmel, M. and Paulssen, H., Noise reduction and detection of weak, coherent signals through phase-weighted stacks. *Geophysical Journal International*, **130**(2), pp.497-505 (1997).
15. Komatitsch, D. & Vilotte, J.P., The spectral-element method: an efficient tool to simulate the seismic response of 2D and 3D geological structures, *Bull. seism. Soc. Am.,* **88,** 368–392 (1998).
16. Komatitsch, D., Ritsema, J. & Tromp, J., The spectral-element method, Beowulf computing, and global seismology, *Science,* **298,** 1737–1742 (2002).
17. Tsuboi, S., D. Komatitsch, C. Ji, and J. Tromp, Broadband modeling of the 2002 Denali Fault earthquake on the Earth Simulator. *Phys. Earth Planet. Inter.***139**, 305–312 (2003).
18. Komatitsch, D., Tsuboi, S. & Tromp, J., The spectral-element in seis- mology, in *Seismic Earth: Array analysis of broadband seismograms,*eds Levander, A. & Nolet, G., *AGU Geophysical Monograph* **157**, AGU, pp. 205–227. (2005)

19. Kustowski, B., Ekström, G. and Dziewoński, A.M., Anisotropic shear-wave velocity structure of the Earth's mantle: A global model. *Journal of Geophysical Research: Solid Earth*, **113**(B6). (2008).
20. Bassin, C., G. Laske, and G. Masters, The current limits of resolution for surface wave tomography in North America, Eos Trans. AGU, **81**, F897 (2000).
21. Vočadlo, L., Ab initio calculations of the elasticity of iron and iron alloys at inner core conditions: evidence for a partially molten inner core? *Earth Planet. Sci. Lett.***254**, 227–232 (2007).
22. Deuss, A., Normal mode constraints on shear and compressional wave velocity of the Earth's inner core. *Earth Planet. Sci. Lett.***268** (3–4), 364–375 (2008).
23. Mao, H.K., Shu, J., Shen, G., Hemley, R.J., Li, B., Singh, A.K., Elasticity and rheology of iron above 220 GPa and the nature of the Earth's inner core. *Nature***396**, 741–743 (1998).
24. Tromp, J., C. Tape, and Q. Liu. Seismic tomography, adjoint methods, time reversal and banana-doughnut kernels. *Geophys. J. Int.*, **160**(1):195–216, (2005). doi: 10.1111/j.1365-246X.2004.02453.x.
25. Tromp, J., D. Komatitsch, and Q. Liu. Spectral-element and adjoint methods in seismology. *Communications in Computational Physics*, **3**(1):1–32, (2008).
26. Liu, Q. and J. Tromp. Finite-frequency kernels based on adjoint methods. *Bull. seism. Soc. Am.*, **96**(6):2383–2397, (2006). doi: 10.1785/0120060041.
27. Liu, Q. and J. Tromp. Finite-frequency sensitivity kernels for global seismic wave propagation based upon adjoint methods. *Geophys. J. Int.*, **174**(1):265–286, (2008). doi: 10.1111/j.1365-246X.2008.03798.x.
28. Tape, C. H., Liu, Q., & Tromp, J., Finite-frequency tomography using adjoint methods -Methodology and examples using membrane surface waves, *Geophys. J. Int.*, **168**, 1105–29 (2007).
29. Tape, C. H., Liu, Q., Maggi, A., & Tromp, J., Adjoint tomography of the southern California crust, *Science*, **325**(5943), 988–992 (2009).
30. Peter, D., D. Komatitsch, Y. Luo, R. Martin, N. Le Goff, E. Casarotti, P. Le Loher, F. Magnoni, Q. Liu, C. Blitz, T. Nissen-Meyer, P. Basini, and J. Tromp. Forward and adjoint simulations of seismic wave propagation on fully unstructured hexahedral meshes. Geophys. J. Int., 186(2):721–739, (2011). doi: 10.1111/j.1365-246X.2011.05044.x.
31. Ekström, G., M. Nettles, and A. M. Dziewonski, The global CMT project 2004-2010: Centroid-moment tensors for 13,017 earthquakes, *Phys. Earth Planet. Inter.*, **200-201**, 1-9 (2012) doi:10.1016/j.pepi.2012.04.002.
32. Stroujkova, A., and V. F. Cormier, Regional variations in the upper-most 100 km of the Earth's inner core, *J. Geophys. Res.*, **109**, B10307, (2004) doi:10.1029/2004JB002976
33. Leyton, F., Koper, K.D., Zhu, L. and Dombrovskaya, M., On the lack of seismic discontinuities within the inner core. *Geophysical Journal International*, **162**(3), pp.779-786 (2005).
34. Yu, W.C. and Wen, L., Seismic velocity and attenuation structures in the top 400 km of the Earth's inner core along equatorial paths. *Journal of Geophysical Research: Solid Earth*, **111**(B7) (2006).

35. Cormier, V.F., Attanayake, J. and He, K., Inner core freezing and melting: Constraints from seismic body waves. *Physics of the Earth and Planetary Interiors*, **188**(3-4), pp.163-172 (2011).
36. Cormier, V.F. and Stroujkova, A., Waveform search for the innermost inner core. *Earth and Planetary Science Letters*, **236**(1-2), pp.96-105 (2005).
37. Tanaka, S. and Hamaguchi, H., Degree one heterogeneity and hemispherical variation of anisotropy in the inner core from PKP (BC)–PKP (DF) times. *Journal of Geophysical Research: Solid Earth*, **102**(B2), pp.2925-2938 (1997).
38. Ishii, M., and A. M. Dziewonski, The innermost inner core of the Earth: Evidence for a change in anisotropic behavior at the radius of about 300 km, *Proc. Natl. Acad. Sci. U. S. A.*, **99**, 14,026–14,030, (2002) doi:10.1073/pnas.172508499.
39. Waszek, L. and Deuss, A., Distinct layering in the hemispherical seismic velocity structure of Earth's upper inner core. *Journal of Geophysical Research: Solid Earth*, **116**, B12313 (2011).
40. Finlay, C.C., Kloss, C., Olsen, N. et al. The CHAOS-7 geomagnetic field model and observed changes in the South Atlantic Anomaly. *Earth Planets Space***72**, 156 (2020). https://doi.org/10.1186/s40623-020-01252-9

Figures

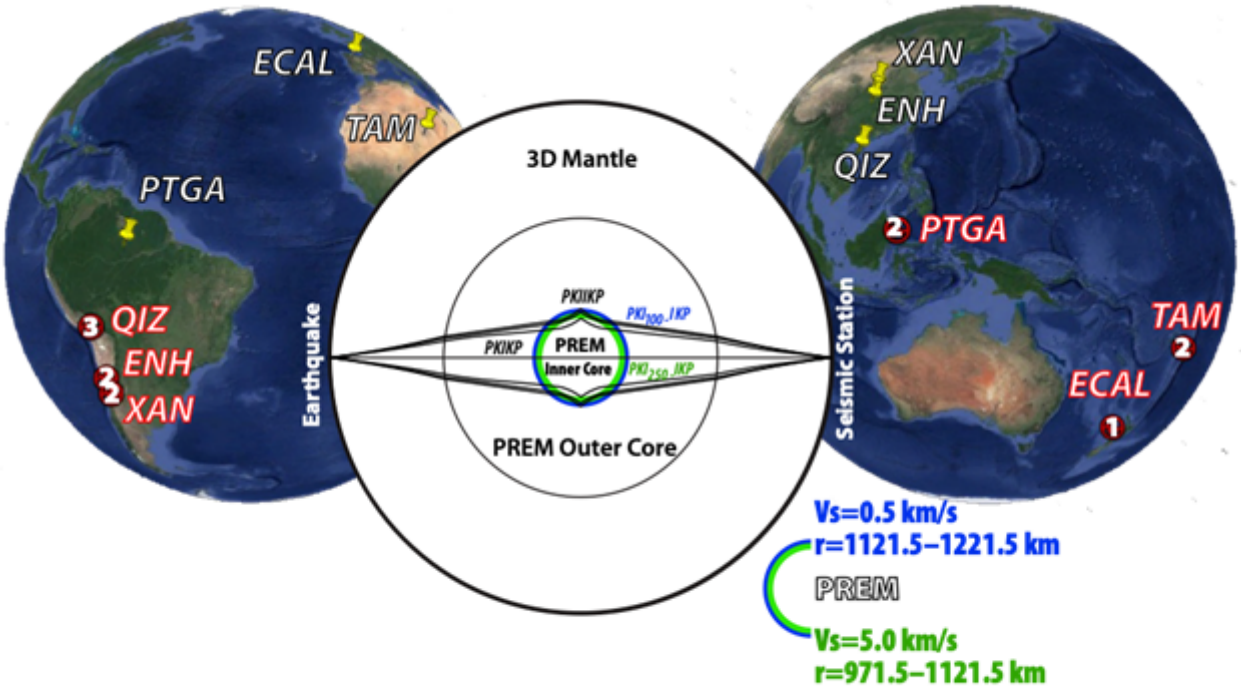

Figure 1

Maps show the locations of earthquakes (red symbols) and corresponding antipodal stations (red outlined). The white numeral at the earthquake symbol indicates the number of events analyzed for the antipodal path. Locations of the antipodal seismic stations are labeled (yellow pins). Inset figure shows the antipodal ray paths (black) for PKIKP, PKIIKP and the paths for the central core phases, PKI_{100}-IKP and PKI_{250}-IKP . Path segments propagating in a 3D Mantle, PREM Outer Core, and a PREM central Inner Core, are designated P, K, and I, respectively. Whereas PKIIKP reflects beneath the Inner Core Boundary, PKI_{100}-IKP reflects beneath an interface in the upper inner core, demarcated by the blue circle above 100 km depth. Similar, PKI_{250}-IKP reflects beneath an interface in the upper inner core, demarcated by the green circle between 100 and 250 km depth within the Inner Core. The starting model replaces the PREM shear velocity by a 0.5 km/s blue layer, and 5.0 km/s green layer. Although ray paths are shown in this cross-section, the antipodal energy converges from all azimuths as a ray surface.

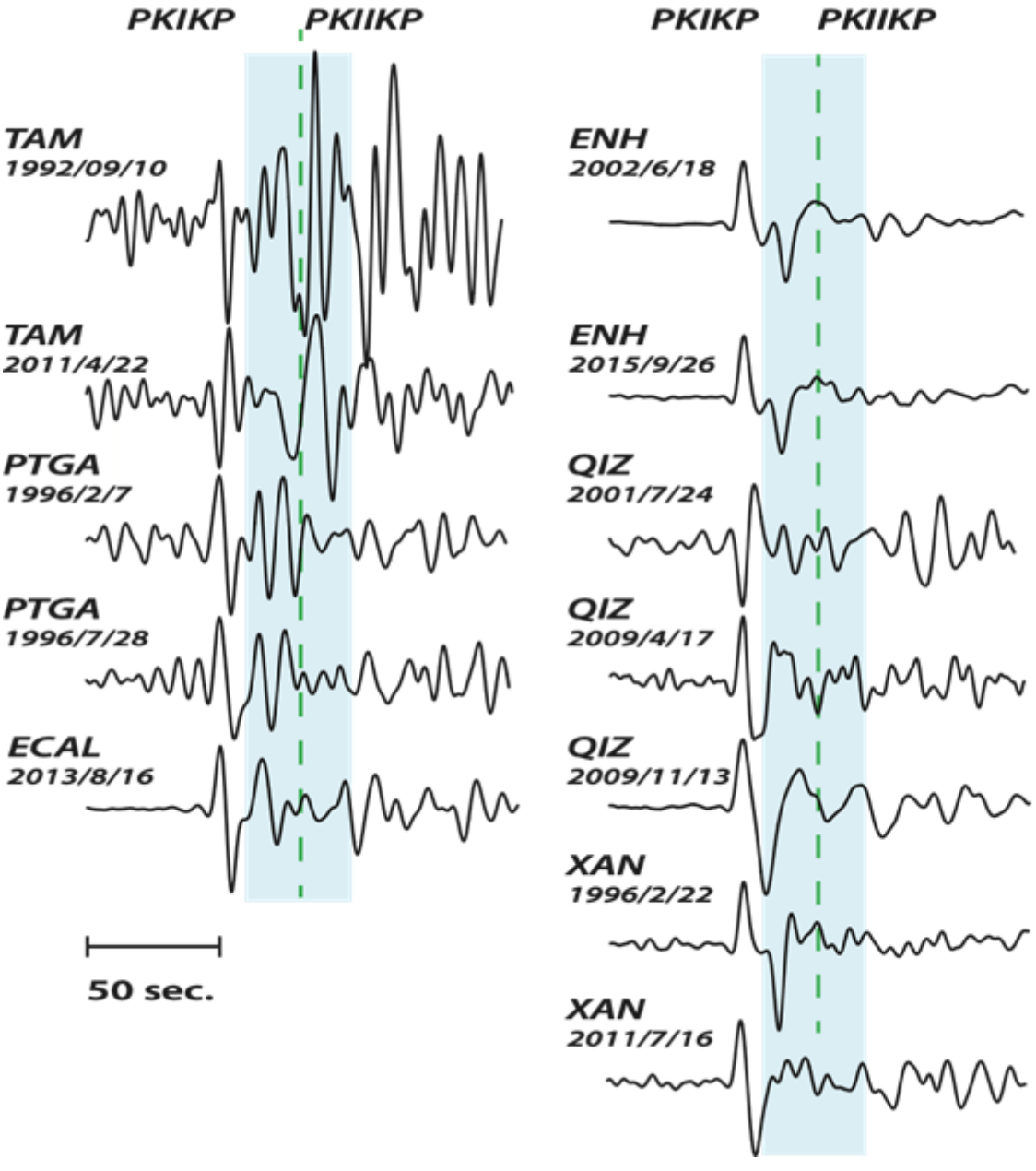

Figure 2

Observed vertical antipodal broadband seismograms (> 179°) are shown for twelve earthquake-receiver pairs, which are used to derive the sensitivity kernel for the shear wave velocity structure on the inner core surface. Time and amplitude are normalized by the arrival of PKIKP. In the analysis both data and SEM are identically bandpass filtered between 50 and 8 sec. The timing of the inner core phase PKIIKP is indicated (dashed green line). The light blue shading approximates the time interval used to calculate the adjoint source. We note that the 1992/9/10 TAM event is one of three nearly identical events discussed in Butler and Tsuboi (2010) and Tsuboi and Butler (2020).

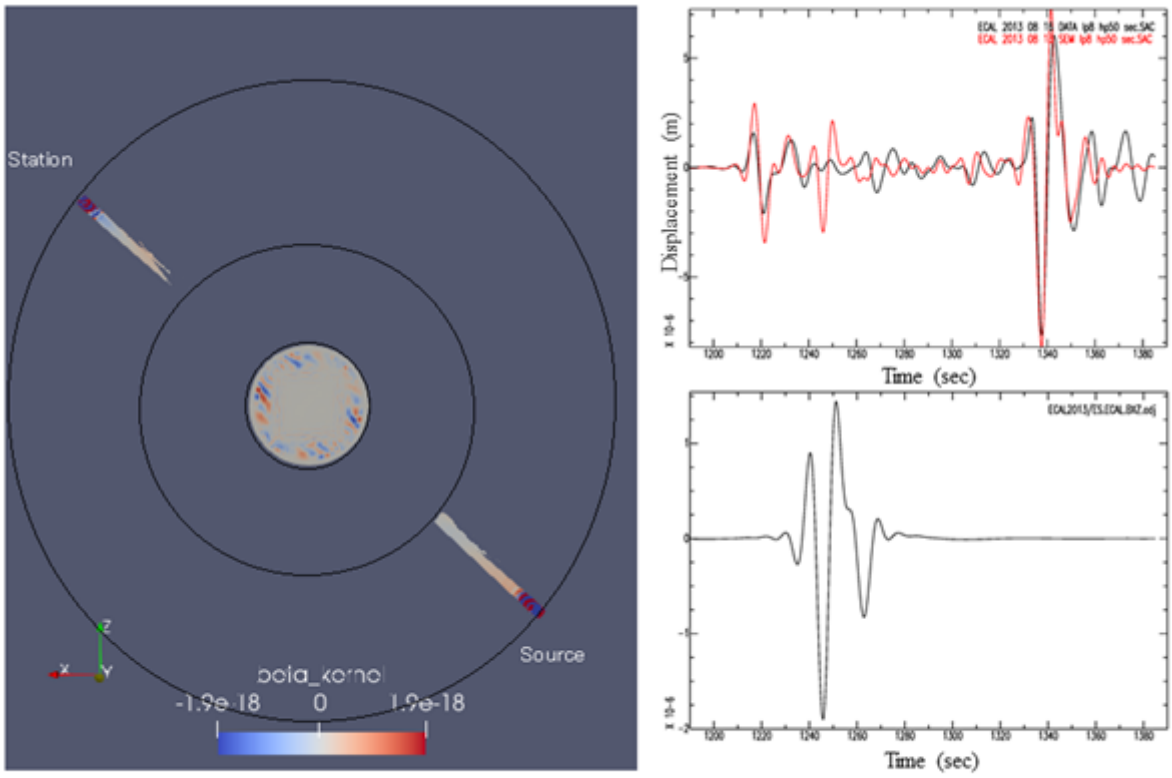

Figure 3

(left) A cross-sectional view of the sensitivity kernel of the shear wave velocity structure of the amplitude with respect to the PKIIKP and PKI_{100}-IKP wave is shown.(upper right) The theoretical seismic waveform (red) and the observed waveform (black) for the August 16, 2013 earthquake in New Zealand observed at the ECAL station in Spain, and (lower right) the adjoint source of the amplitude for the PKIIKP and PKI_{100}-IKP waves. These traces are ground displacement and bandpass filtered between periods 8 second and 50 second.

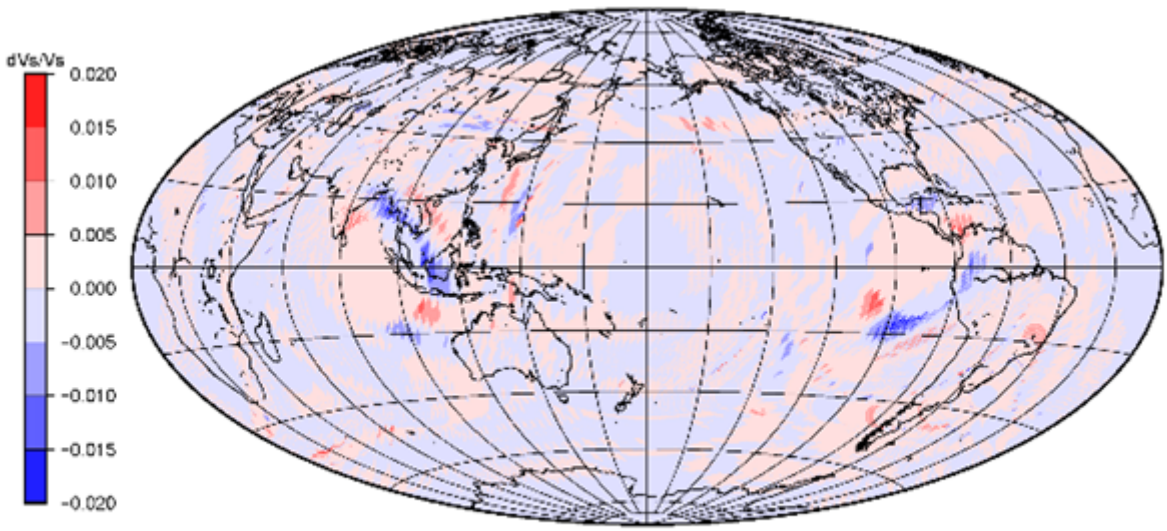

Figure 4

Map of percentage of shear velocity modification to be made to the initial model. This corresponds to the modification to the model from a depth of 100km to the surface of the inner core.

Supplementary Files

This is a list of supplementary files associated with this preprint. Click to download.

- TableS1.docx